I&EC research
Industrial & Engineering Chemistry Research

Article

pubs.acs.org/IECR

Ethanol Oxidative Steam Reforming over Rh(1%)/$MgAl_2O_4$/Al_2O_3 Catalyst

Cecilia Graschinsky, Jorgelina Lupiano Contreras, Norma Amadeo, and Miguel Laborde*

Laboratorio de Procesos Catalíticos, Departamento de Ingeniería Química, Facultad de Ingeniería, UBA, Pabellón de Industrias, Ciudad Universitaria, (1428) Buenos Aires, Argentina

Supporting Information

ABSTRACT: The ethanol oxidative steam reforming reaction was studied over a rhodium-based catalyst that was prepared by wet impregnation method. The oxygen-to-ethanol ratio (R_o = 0−1.2), space time (τ_{Et} = 15−45 g_{cat}·min/mol_{Et}), and temperature (T = 673−873 K) were varied to determine the reaction scheme. The catalyst showed excellent selectivity for the production of hydrogen and a very good stability. A network of eight reactions was used: ethanol decomposition and steam reforming; water gas shift; methane steam reforming; and ethanol, methane, carbon monoxide, and hydrogen oxidations. The obtained results suggest that the oxidation reactions predominate in the first part of the reactor and at low temperatures. Ethanol partial oxidation was also studied, and the same reaction scheme was found for this reaction when varying R_o (0.25−1.0), τ_{Et}(9.5−45.8 g_{cat}·min/mol_{Et}) and T (573−673 K). Finally, a reaction mechanism of 22 elementary steps was proposed, and the kinetic parameters were obtained.

1. INTRODUCTION

Hydrogen is an essential raw material for the chemical, petrochemical, oil, and iron and steel industries.[1] In recent years; hydrogen has become more interesting because of its application as an energy vector. If produced from renewable sources, it may also contribute to the production of sustainable energy because it can be directly converted electrochemically in proton exchange membrane fuel cells to produce electricity used in transportation applications and portable power devices. Hydrogen can be produced through the steam reforming of biomass-derived liquids such as bioethanol, a water and ethanol mixture that is obtained mainly by biomass fermentation.[2] In addition to being a renewable raw material, ethanol presents other advantages: it is almost nontoxic and possesses a high content of hydrogen in its molecule. Ethanol steam reforming (SR) R1 is a strong endothermic process, and (ideally) only CO_2 and H_2 are produced. However, nondesirable products appear during hydrogen production, such as CH_4, CO, C_2H_4O, and C_2H_4.[3,4] Because of the strong endothermicity of the process, a great amount of energy must be provided. Heat could be supplied externally (using the same alcohol as a fuel in a burner) or pure oxygen (or air) could be fed to the reforming reactor to burn a portion of the ethanol.[5−7] To achieve thermal neutrality, 0.61 mol of oxygen per mole of ethanol must be fed. This process is known as autothermal reforming of ethanol or oxidative steam reforming (OSR) (R2).

$$C_2H_5OH(l) + 3H_2O(l) \rightarrow 2CO_2(g) + 6H_2(g) \quad H = 347\ kJ/mol \qquad (R1)$$

$$C_2H_5OH(l) + 1.78H_2O(l) + 0.61O_2(g) \rightarrow 2CO_2(g) + 4.78H_2(g) \quad \Delta H = 0 \qquad (R2)$$

Because the system involves multiple reactions,[8] the hydrogen yield can be affected by the operating conditions. With the intention of obtaining a first approximation to the system, our group carried out a detailed thermodynamic study of the OSR using the Gibbs energy minimization method.[9] It was found that the addition of oxygen in the feed discourages H_2 and CO production. Nevertheless, carbon formation also decreases as O_2 in the feed increases. On the other hand, Wang and Wang[10] found that temperatures from 973 to 1173 K and oxygen−ethanol ratios from 0.6 to 0.8 ensure optimal conditions for oxidative steam reforming.

Regarding the catalyst, it must be pointed out that no commercially viable catalysts for ethanol SR or OSR are currently available. The literature shows that the catalysts used for OSR are essentially the same as those used for SR.[11−21] Cavallaro et al.[11] studied the OSR with the same catalyst (Rh (5%)/Al_2O_3) with which they had worked on SR. These authors found that at 923 K and a water−ethanol ratio of 12.6, the addition of oxygen in the feed produces a maximum performance of hydrogen for an oxygen−ethanol ratio of 0.6. The authors also found that, in the experimental conditions used in their work, the water gas shift (WGS) reaction is in equilibrium.

Salge et al.[12] studied the OSR with catalysts based on noble metals, such as Rh, Pt, Pd and Ru, on different supports. The authors analyzed the effect of adding oxygen in the feed at 973 K and found that for Rh/CeO_2/Al_2O_3 catalysts, the moles of hydrogen produced per mole of ethanol fed decreased with the addition of oxygen. It was further observed that a Pt catalyst is unstable at low oxygen-to-ethanol ratios, and Pd loses activity due to coke formation. Furthermore, the authors found that the

Special Issue: Alírio Rodrigues Festschrift

Received: January 31, 2014
Revised: April 20, 2014
Accepted: May 7, 2014
Published: May 7, 2014

   dx.doi.org/10.1021/ie500445u | *Ind. Eng. Chem. Res.* 2014, 53, 15348−15356

Rh−Ce catalyst was the most active and selective to hydrogen, showing a maximum in hydrogen selectivity (80%) at an oxygen−ethanol ratio of 0.6. Biswas and Kunzru[13] employed a $Ni/CeO_2–ZrO_2$ catalyst using a water−ethanol molar ratio of 8.0. These authors found that, in the absence of oxygen, the ethanol conversion reached 100% at temperatures above 923 K, whereas when the oxygen−ethanol ratio in the feed is increased to 1.0, complete conversion is obtained at substantially lower temperatures (673 K). They also calculated the OSR heat of reaction at 923 K (for different oxygen−ethanol ratios) and concluded that the addition of oxygen is desirable, allowing for greater efficiency without sacrificing performance (total hydrogen obtained). Unlike Cavallaro et al.,[11] Biswas and Kunzru[13] found that at 923 K and an oxygen−ethanol ratio of 0.5, the WGS reaction is not in equilibrium. It must be noted that Cavallaro et al. used a Rh-based catalyst that is known as a good WGS catalyst, and the latter authors employed a Ni-based catalyst.

Fierro et al.[14] compared the behavior of 20% Ni and 5% Rh (both supported on Al_2O_3 on the OSR). They found that at high temperatures (923−1073 K), a water−ethanol ratio of 1.6 and an oxygen−ethanol ratio of 0.68, the Rh catalyst enables higher H_2 production. Liguras et al.[15] worked on a Ni catalyst ($Ni(13\%)/La_2O_3$) and studied the temperature profile along the reactor. The authors found a temperature peak at the inlet and subsequently a temperature decrease along the reactor. From this information, they concluded that the oxidation reactions occur at the reactor's inlet, and the endothermic reforming reaction follows.

The overall objective of this work is to study the oxidative steam reforming reaction of ethanol using $Rh(1\%)/MgAl_2O_4/Al_2O_3$ as a catalyst. In a previous work, our group studied the ESR using the same catalyst, and the following reaction scheme was proposed for ESR:

$$C_2H_5OH \rightarrow CO + CH_4 + H_2 \quad (R3)$$

$$C_2H_5OH + H_2O \rightarrow CO_2 + CH_4 + 2H_2 \quad (R4)$$

$$CO + H_2O \leftrightarrow CO_2 + H_2 \quad (R5)$$

$$CH_4 + H_2O \leftrightarrow CO + 3H_2 \quad (R6)$$

Kinetic parameters of each reaction were also reported.[22]

The specific objective of this work is to determine the reaction scheme in the OSR and estimate the kinetic parameters of the reactions involved. To achieve this goal, the effect of temperature, the ethanol-to-oxygen ratio, and space time on the conversion and product distribution was studied. The effect of temperature and space time in the partial oxidation of ethanol using the same catalyst was taken into account in the analysis.

2. EXPERIMENTAL SECTION

2.1. Catalyst. Catalytic experiments were carried out using a supported catalyst $Rh(1\%)MgAl_2O_4/Al_2O_3$ prepared by the "Catalysis for Metals" team at University of Poitiers. The complete experimental procedure was described in detail by Aupetre et al.[23]

Fresh catalyst was characterized by H_2 chemisorption and sorptometry (S_{BET}). The BET surface area was obtained using Micromeritics ASAP 2020 equipment. The reduced Rh area, metal dispersion, and particle size were evaluated by H_2 chemisorption assuming a Rh/H = 1 stoichiometry and a mean area of 7.52 Å^2 per Rh atom. H_2 chemisorption analysis was carried out using Micromeritics Autochem II 2920 equipment. The fresh catalyst was prereduced under a H_2/Ar flow (50%) with a temperature ramp of 10 K/min from ambient temperature to 973 K.

2.2. Catalytic Runs. The kinetic measurements were carried out in conventional flow laboratory equipment. A quartz reactor (4 mm internal diameter), where the catalytic bed was placed, was located in an electrical oven. The reaction temperature was monitored using a thermocouple placed inside the catalytic bed. The ethanol (Merck)/water mixture was fed as a liquid with a syringe pump. The mixture was evaporated in an electrical heater (623 K) before entering the reactor and diluted with an Ar stream. Air was added into the inlet stream just before the reactor to avoid interference from possible homogeneous reactions. The catalyst was grounded to give a 44−88 μm diameter range to avoid internal diffusion effects and diluted with inert material (SiC) of the same diameter to avoid temperature gradients inside the catalytic bed. The liquid flow was 0.04 mL/min, and the reaction temperature was varied between 673 and 873 K. The space time (eq 1) was changed by modifying the mass of catalyst between 4 and 12 mg.

Prior to catalytic evaluation, experiments were carried out to verify that contributions of homogeneous phase reaction were negligible and to ensure the absence of external and internal diffusion control on the reaction rate. Results showed that the use of catalyst particles of diameter smaller than 88 μm and a total volumetric flow over 390 mL/min guaranteed chemical control.

Prior to reaction, the catalyst was reduced in situ under a H_2 flow of 50 mL/min at 773 K for 1 h. The temperature rise from ambient to 773 K was programmed at 10 K/min and, after 1 h of H_2 stream, was changed to N_2 flow of 100 mL/min at reaction temperature for 30 min.

The analysis of the feed and product streams was carried out online by gas chromatography in an Agilent chromatograph, model GC 6820, with two columns (Innowax and Carbonplot) and FID and TCD detectors.

The steady state condition was reached after approximately 1 h of reaction. The reproducibility of experimental results was checked, and the experimental error was <2%. The carbon balance was above 95% in all experiments, which corroborates the following two observations: no carbon formation was detected, and the catalyst exhibited stable performance over an 8−12 h period.

The catalytic results are discussed in terms of ethanol (eq 2) and water (eq 3) conversions, CO_x and methane yields (eq 4), hydrogen yield (eq 5), and selectivity (eq 6); where F_i^0 and F_i are the molar flow of the ith component in the inlet and outlet streams, respectively, and W is the catalyst mass.

$$\tau_{Et} = \frac{W}{F_{Et}^0} \quad (1)$$

$$X_{Et} = \frac{F_{Et}^0 - F_{Et}}{F_{Et}^0} \times 100 \quad (2)$$

$$X_{H_2O} = \frac{F_{H_2O}^0 - F_{H_2O}}{F_{H_2O}^0} \times 100 \quad (3)$$

$$Y_j = \frac{F_j}{2F_{et}^0} \times 100 \qquad j = CO_x, CH_4 \quad (4)$$

dx.doi.org/10.1021/ie500445u | Ind. Eng. Chem. Res. 2014, 53, 15348−15356

$$Y_{H_2} = \frac{F_{H_2}}{F_{Et}^0} \quad (5)$$

$$S_{H_2/H_2O} = \frac{F_{H_2/H_2O}}{3(F_{et}^0 - F_{et})} \times 100 \quad (6)$$

3. RESULTS AND DISCUSSION

The characteristics of the fresh catalyst are summarized in Table 1.

Table 1. Characteristics of Fresh Catalyst

BET surface area (m^2/g)	95.43
pore volume (cm^3/g)	0.28
pore size (Å)	115.87
metal dispersion (%)	57.20
metallic surface area (m^2/g)	2.52
particle diameter (nm)	1.92

3.1. Effect of Oxygen–Ethanol Ratio (R_o). To evaluate the effect of R_o on the product distribution, the air flow rate fed to the reactor was varied. The argon flow rate was modified in each experiment to keep the space time and the mole fractions of ethanol and water in the gas phase constant. In Table 2,

Table 2. Ethanol and Water Conversion and Hydrogen Selectivity and Yield vs R_o[a]

R_o	X_{Et}	X_{H_2O}	S_{H_2}	Y_{H_2}
0	80.0	35.0	152.7	3.9
0.3	82.6	30.5	137.7	3.8
0.6	85.7	26.0	117.3	3.5
0.9	91.7	22.4	111.1	3.3
1.2	100.0	15.3	105.3	3.0

[a] T = 873 K; R = 5.5; τ_{Et} = 23 g_{cat}·min/mol^0_{et}.

ethanol and water conversion and yield and selectivity of hydrogen vs R_o are shown. The results show that in the absence of oxygen, ethanol conversion is 80%, and total conversion is attained when R_o is equal to 1.2. For R_o values less than 0.6, ethanol conversion increases slightly (remaining close to 80%). It must be noted that the hydrogen yield decreases with R_o, although ethanol conversion increases. Water conversion decreases sharply (around 50%) with the addition of oxygen into the feed. The reduction in H_2 selectivity as R_o increases indicates that the contribution of reactions that produce H_2 decreases. Cavallaro et al.,[11] working with a rhodium-based catalyst at 923 K and different steam-to-ethanol ratios, report that the hydrogen yield first increases and then decreases when the oxygen concentration in the feed increases. Our results indicate that the yield of hydrogen decreases as R_o increases in the whole range studied.

The CO, CO_2, and CH_4 yields vs R_o are shown in Figure 1. Results indicate that the CO yield decreases slightly when R_o increases, whereas the CO_2 yield increases more sharply. The CH_4 yield remains practically unchanged as R_o changes.

The study on ethanol steam reforming[16] (SR) using the same catalyst has reported reactions such as ethanol decomposition (R3), ethanol steam reforming (R4), WGS (R5), and methane steam reforming (R6).

Ethanol decomposition (R3) occurs via dehydrogenation to acetaldehyde (R7) and its subsequent decomposition (R8).

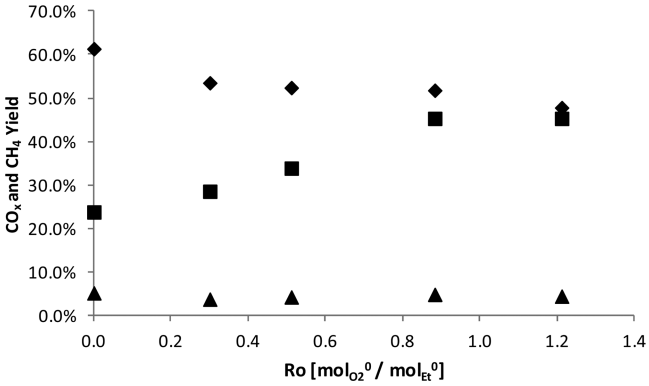

Figure 1. Yield as a function of R_o. T = 873 K, τ_{Et} = 23 g_{cat}·min/mol_{Et}, R = 5.5. ♦, CO; ■, CO_2; ▲, CH_4.

Because these reactions occur very rapidly, acetaldehyde appears only as trace amounts and only under particular operating conditions.

$$C_2H_5OH \rightarrow C_2H_4O + H_2 \quad (R7)$$

$$CH_3CHO \rightarrow CO + CH_4 \quad (R8)$$

The increase in ethanol conversion when R_o increases (Table 2) can be explained by the occurrence of ethanol partial oxidation to acetaldehyde and water (R9) due to the addition of oxygen into the system.

$$C_2H_5OH + \frac{1}{2}O_2 \rightarrow CH_3CHO + H_2O \quad (R9)$$

Methane is produced by C_2H_4O decomposition (R8) and consumed by the SMR (R6). With the addition of O_2, the dehydrogenation (R7) and oxidation (R9) of ethanol contribute to the formation of C_2H_4O, which decomposes to CH_4. However, the results show that the increase in C_2H_4O production due to increased ethanol conversion does not result in an increase in the CH_4 yield. This is because CH_4 is consumed by SMR (R6), producing more CO and H_2. In addition, CH_4 partial oxidation (R10) cannot be dismissed. Under these hypotheses, the increase in O_2 concentration in the feed should cause an increase in the yields of CO and H_2.

CO would be produced by SMR (R6), C_2H_4O decomposition (R8), and CH_4 partial oxidation (R10) reactions, and H_2 would form via WGS (R5), SMR (R6), ethanol dehydrogenation (R7), and CH_4 partial oxidation (R10). However, it should be noted that (1) the H_2 yield decreases with increasing O_2, thus suggesting its consumption via oxidation to H_2O (R11); and (2) CO yield decreases with the addition of O_2, indicating its consumption via WGS reaction (R5), increasing the CO_2 performance. In addition, the oxidation of CO (R12) could not be excluded. These reactions explain the strong increase in the CO_2 yield.

$$CH_4 + \frac{1}{2}O_2 \rightarrow CO + 2H_2 \quad (R10)$$

$$H_2 + \frac{1}{2}O_2 \rightarrow H_2O \quad (R11)$$

$$CO + \frac{1}{2}O_2 \rightarrow CO_2 \quad (R12)$$

dx.doi.org/10.1021/ie500445u | Ind. Eng. Chem. Res. 2014, 53, 15348−15356

The net heat of reaction (ΔH) at a given temperature is a function of the O_2 mole fraction in the feed (eq 7), and it can be evaluated from[24]

$$\Delta H = \sum_j y_j h_j - \sum_j y_j^0 h_j \quad (7)$$

where h_j is the heat of formation of the jth substances at the working temperature, and y_j and y_j^0 are the molar fractions for the substance j at the reactor outlet and inlet stream, respectively.

Using this equation, the net heat of reaction is zero at R_o = 0.7. Cavallaro et al.[11] obtained a similar result. Thus, a value close to 0.7 may be an optimum R_o value (from the energetic viewpoint) with acceptable hydrogen yields.

3.2. Effect of Space Time. The space time was changed by varying the mass of catalyst. All other variables—volumetric flow, feed composition, and temperature—were kept constant. Table 3 shows ethanol conversion, hydrogen yield, and hydrogen selectivity vs space time. Because ethanol is the reactant and hydrogen is the final product, both ethanol conversion and hydrogen yield increase with space time. The larger values (i.e., >100) of the selectivity to H_2 indicate that the reactions that consume water become predominant in the system.

Table 3. Ethanol Conversion, H_2 Yield, and H_2 Selectivity vs Space Time[a]

τ_{Et} (g_{cat}·min/mol_{Et})	X_{Et}	Y_{H_2}	S_{H_2}
15	82.6	2.7	104.5
23	85.7	3.5	117.3
29	96.0	3.6	119.6
44	100.0	3.7	121.2

[a] T = 873 K, R = 5.5, R_o = 0.6.

CO, CO_2, and CH_4 yield vs space time are presented in Figure 2. The CO yield shows a typical "intermediate compound" behavior. The CO_2 yield, in turn, increases throughout the space time range studied confirming that it is a final product. Although the CH_4 yield is very low, it can be seen that it declines with space time. This result is in agreement with previous ones, which allow us to suggest a greater preponderance of reforming reactions on the oxidation reactions set at high space times. With respect to acetaldehyde (results not shown), trace amounts are observed only at low space times. This result is consistent with those published by other authors,[15,25] who found that the oxidation reactions occur in the first part of the reactor, whereas reforming reactions occur at high space times.

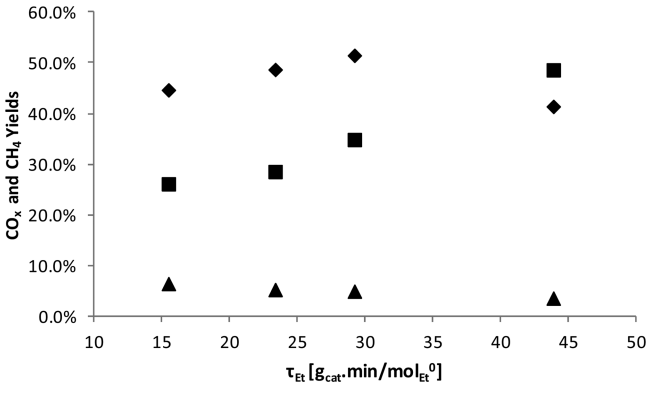

Figure 2. Yield as a function of space time. T = 873 K, R_o = 0.6, R = 5.5. ♦, CO; ■, CO_2; ▲, CH_4.

3.3. Effect of Temperature. Ethanol conversion and H_2 yield increase with temperature (Figure 3) Ethanol conversion reaches 90% at 873 K. At the lowest analyzed temperature (673 K), ethanol conversion is significant (40%), although for these same conditions, H_2 production is negligible. This same figure shows negative conversion values for water (T < 773 K), indicating net formation of water for these conditions. These results suggest that, at lower temperatures, the ethanol oxidation predominates (R9) and hydrogen oxidation could not be ruled out (R11).

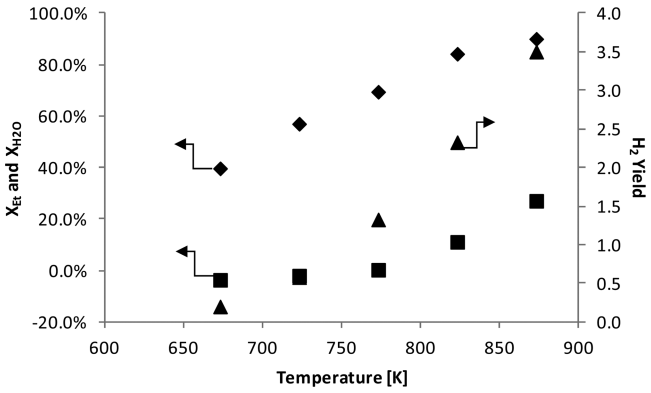

Figure 3. X_{Et}, X_{H_2O}, and H_2 yield as a function of temperature. R_o = 0.6, R = 5.5, τ_{Et} = 23 g_{cat}·min/mol_{Et}. ♦, X_{Et}; ■, X_{H_2O}; ▲, Y_{H_2}.

Yields for CO, CO_2, and methane as a function of temperature are presented in Figure 4. It can be seen that the CO yield increases as the temperature rises because CO-generating reactions (ethanol decomposition (R3) and SMR (R6)) are favored by an increase in temperature. CO_2 is produced by the WGS (R5), but below 773 K, the CO_2 yield increases slightly from presumably the CO oxidation reaction (R12). The strong increase shown by the CO_2 yield at higher temperatures is explained by the greater importance of the WGS reaction (R5). Because CO is consumed in this reaction, a reduction in the rate of increase in its yield, as seen in Figure 5, is expected. Increasing the temperature decreased the CH_4 yield over the entire studied temperature range because it is

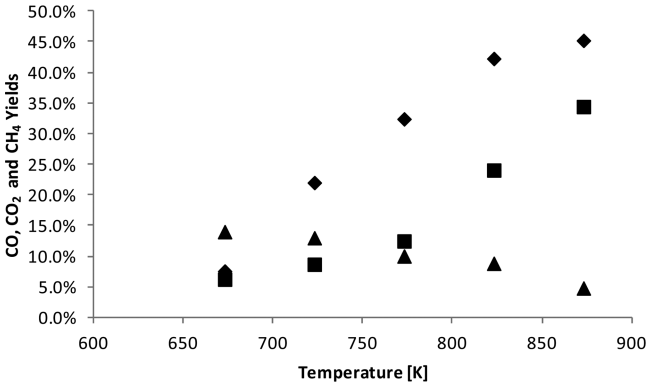

Figure 4. Yield as a function of temperature. τ_{Et} = 23g_{cat}·min/mol_{Et}, R_o = 0.6, R = 5.5. ♦, CO; ■, CO_2; ▲, CH_4.

dx.doi.org/10.1021/ie500445u | Ind. Eng. Chem. Res. 2014, 53, 15348−15356

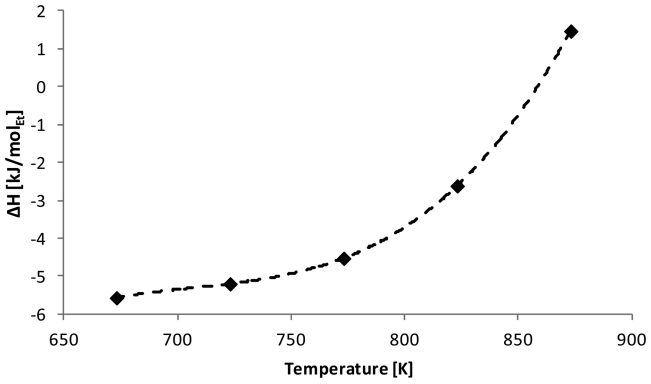

Figure 5. Reaction heat as a function of temperature. R = 5.5; R_o = 0.6; τ_{et} = 23 g_{cat}·min/mol^0_{Et}.

consumed by SMR (R6). The consumption of CH_4 is more significant at temperatures above 723 K (Figure 4), the temperature from which SMR is thermodynamically possible. The latter, combined with the low CH_4 yield below 723 K, confirms the presence of the CH_4 partial oxidation reaction (R10). For these experimental conditions (R_o = 0.6 and R = 5.5), oxidation reactions predominate at temperatures between 673 and 773 K, and above 823 K, the steam reforming reactions prevail.

Heat of reaction, evaluated from eq 7 vs temperature is shown in Figure 5. Working at R_o = 0.6, the process is exothermic if the temperature is below 860 K. If the reactor is operated above this temperature, the process requires an energy input.

The reaction scheme proposed for the ethanol oxidative reforming reaction on a $Rh(1\%)/MgAl_2O_4/Al_2O_3$ catalyst is given in reactions R3−R6 and R9−R12. Results have indicated that the influence of each subgroup of reactions (oxidation reactions R9 and R12 and reforming reactions R3 to R6) depends on the operating conditions chosen for the reactor.

3.4. Partial Oxidation of Ethanol (EPO). Considering that the oxidation reactions are predominant at lower temperature and space time, the ethanol partial oxidation using the same catalyst was carried out to analyze the product distribution. The operating conditions that were used to analyze the effect of temperature on the conversion and product distribution in the EPO were y^0_{et} = 0.022, $y^0_{O_2}$ = 0.013, τ = 14.3 g_{cat}·min/mol_{et}, and T = 623−673 K. Ethanol and oxygen conversions (results not shown) exhibit behavior typical for reactive, increasing as the temperature increases. The main reaction products are CO, CO_2, CH_4, H_2, and H_2O; their yields also increase with temperature (Figure 6). CO and CH_4 are produced by ethanol oxidation (R9), followed by ethanol decomposition (R3) both of which are favored by temperature. CO_2 production can be due to the methane oxidation (R10) as that CO oxidation (R12). The ethanol reforming reaction (R4) favors an increase in the CO_2, CH_4, and H_2 yields with increasing the reaction temperature. Hydrogen is formed, in principle, by ethanol decomposition (R3) and water is produced by the ethanol oxidation (R9). Water formation may be favoring the WGS reaction (R5), which is also contributed to H_2 formation.

The operating conditions that were used to analyze the effect of space time were y^0_{et} = 0.016, $y^0_{O_2}$ = 0.012, Q_T = 470 mL/min, T = 573 K, and W = 3−14.2 mg_{cat}. Ethanol and oxygen conversions behave as expected, increasing as the residence time increases, oxygen conversion being greater than that of

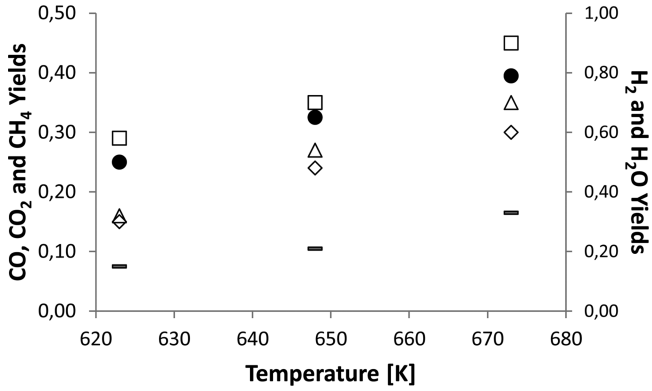

Figure 6. Yields vs temperature. R_o = 0.6; τ_{et} = 14.3 g_{cat}·min/mol^0_{Et}. ◊, CO; □, CO_2; Δ, CH_4; —, H_2; ●, H_2O.

ethanol in the whole range. For the longer space time, O_2 conversion is over 90%, and that of ethanol reaches 60% (Figure 7).

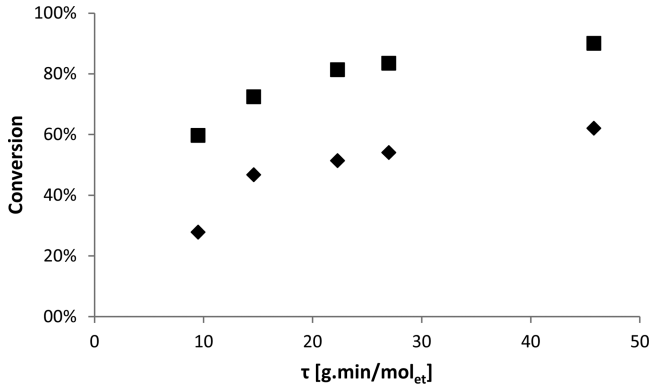

Figure 7. Conversion vs space time. T = 573 K, R_o = 0.75. ♦, X_{Et} ■; X_{O_2}.

The CO, CO_2, and CH_4 yields vs space time are shown in Figure 8. All show a behavior of the final product. As already mentioned, the high yield of CO_2 may be due to oxidation reactions R10 and R12 but also to the WGS reaction, R5.

When comparing H_2 selectivity with H_2O selectivity (Table 4), it can be seen that the first is less than the second and also that their sum is <1 over the range of conditions studied. This indicates that other reactions involving these species are taking

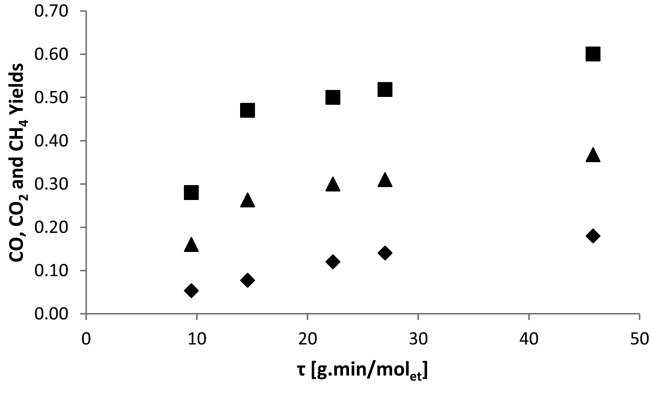

Figure 8. Yields vs space time. T = 573 K, R_o = 0.75, τ_{et} = 14.3 g_{cat}·min/mol^0_{Et}. ♦, CO; ■, CO_2; ▲, CH_4.

dx.doi.org/10.1021/ie500445u | Ind. Eng. Chem. Res. 2014, 53, 15348−15356

Table 4. H_2 and H_2O Selectivities vs Space Time[a]

τ_{Et} (g_{cat}·min/mol_{et})	S_{H_2}	S_{H_2O}
9.5	7.2%	72.0%
14.6	8.6%	50.0%
22.3	11.7%	48.0%
27.0	12.3%	48.1%
45.8	12.6%	44.6%

[a] T = 573 K; R_o = 0.75.

place. If only the ethanol oxidation and decomposition reactions are involved, the sum of both selectivities would be equal to 100%.

In the experiments performed by varying the O_2 concentration in the feed, the presence of methane and CO oxidation reactions (R10, R12) is evident as a result of the decrease of their yields as the O_2 mole fraction is increased (Figure 9). At

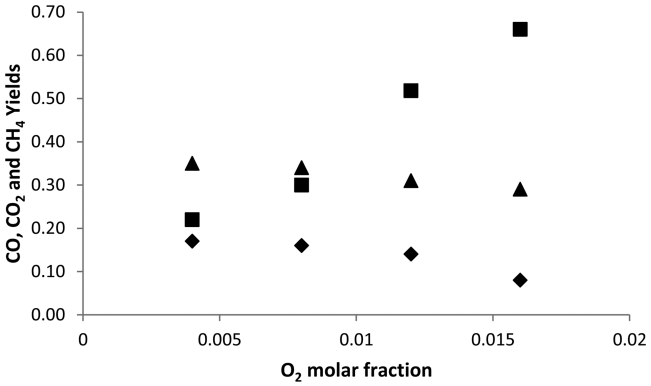

Figure 9. Yield vs O_2 molar fraction. T = 573 K, y^0_{Et} = 0.016, τ_{et} = 27g_{cat}·min/mol_{Et}^0. ♦, CO; ■, CO_2; ▲, CH_4.

the same time, the CO_2 yield increases. On the other hand, the H_2 yield decreases while the H_2O yield increases (Figure 10);

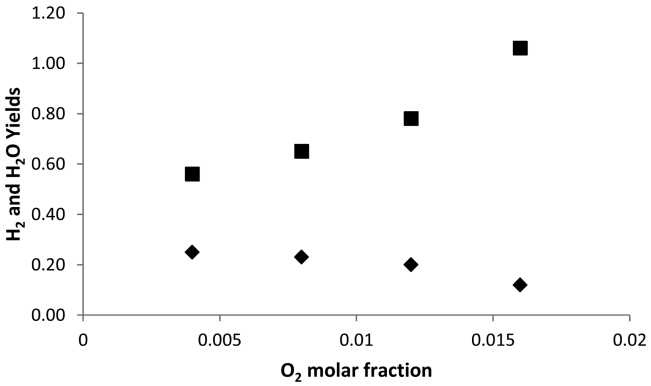

Figure 10. Yield vs O_2 molar fraction. T = 573 K, y^0_{Et} = 0.016, τ_{et} = 27g_{cat}·min/mol_{Et}^0. ♦, H_2; ■, H_2O.

this confirms the presence of the H_2 oxidation reaction (R11). When the effect of space time on the H_2 and H_2O selectivity was analyzed, the presence of at least one reaction that involved these species in addition to the oxidation and decomposition of ethanol was proposed. The H_2 oxidation reaction responds to such behavior.

Experimental evidence indicates that the reaction scheme of EPO would consist of the ethanol, CH_4, H_2, and CO oxidation reactions; ethanol decomposition; ethanol reforming; and WGS reactions. However, when ethanol and O_2 are completely consumed, the system is composed of five species: CO, CH_4, CO_2, H_2, and H_2O. In turn, these five species arise from the proper combination of three atomic species: C, H, and O. Therefore, two linearly independent reactions are necessary to describe the equilibrium toward which the system tends. In summary, it should be noted that there are at least two linearly independent reversible reactions. The WGS is one of them. Because of the low temperature employed in the EPO study, the reforming of CH_4 (R6) is not thermodynamically possible, but its inverse, the CO methanation, is.

The same scheme of eight reactions that had been deduced for OSR is then obtained. Reforming reactions are most important at high temperature; nevertheless, in this case, it will be given less importance than that of the OSR system because available H_2O is formed only from the oxidation reactions. These latter reactions are prevalent throughout the range of operating conditions studied.

3.5. Kinetics. In a previous paper,[22] a kinetic study of ESR was presented, and a reaction mechanism was proposed using the same catalyst.

Only a few papers have analyzed the mechanism of EPO reactions to produce H_2. Most of them used metallic catalysts and supports with redox properties in which O_2 is the oxidant agent of the support and in which a Mars–Van Krevelen type mechanism is proposed.[26−31]

Costa et al.[27] employed a Pd catalyst supported on Y_2O_3 (nonreducible oxide) and on CeO_2 (reducible oxide). With both supports, the authors proposed the same first stages, in agreement with our previous results for ESR:[22] ethanol adsorption and ethoxide formation. This ethoxide is dehydrogenated to C_2H_4O. Nevertheless, using a Pd/Y_2O_3 catalyst, C_2H_4O is not produced,[32−34] but when Pd/CeO_2 is employed, acetaldehyde is observed among the products.[28,30,31,35]

Other authors carried out the methane partial oxidation reaction using Rh supported on nonreducible oxides.[36−38] They propose the dissociative adsorption of oxygen on the metallic Rh, which is the active phase. The adsorbed oxygen species favors the oxidation of CO to CO_2 and H_2 to H_2O.

Taking into account the results obtained with ESR[22] and with EPO in this work, it can be concluded that the mechanism proposed for OSR includes the mechanism proposed for ESR[22] plus five new steps related to the presence of oxygen: dissociative adsorption of oxygen and four reaction steps between the intermediates produced from ethanol decomposition and the adsorbed oxygen. Considering the reaction scheme presented, the mechanism for OSR is as follows:

$$C_2H_5OH + (a) = C_2H_5OH(a) \quad (S1)$$

$$C_2H_5OH(a) + (a) = C_2H_5O(a) + H(a) \quad (S2)$$

$$C_2H_5O(a) + (a) = C_2H_4O(a) + H(a) \quad (S3)$$

$$C_2H_4O(a) + (a) = CH_3(a) + CHO(a) \quad (S4)$$

$$CH_3(a) + (a) = CH_2(a) + H(a) \quad (S5)$$

$$CH_2(a) + (a) = CH(a) + H(a) \quad (S6)$$

$$H_2O + (a) = H_2O(a) \quad (S7)$$

$$H_2O(a) = HO(a) + H(a) \quad (S8)$$

dx.doi.org/10.1021/ie500445u | Ind. Eng. Chem. Res. 2014, 53, 15348−15356

$$CHO(a) + (a) = CO(a) + H(a) \quad RDS_1 \tag{S9}$$

$$CHO(a) + HO(a) = CO_2(a) + H_2 + (a) \quad RDS_2 \tag{S10}$$

$$CO(a) + HO(a) = CO_2(a) + H(a) \quad RDS_{WGS} \tag{S11}$$

$$CH(a) + HO(a) = CO(a) + H_2 + (a) \quad RDS_{SMR} \tag{S12}$$

$$CH_4(a) + (a) = CH_3(a) + H(a) \tag{S13}$$

$$H_2 + 2(a) = 2H(a) \tag{S14}$$

$$CH_4 + (a) = CH_4(a) \tag{S15}$$

$$CO + (a) = CO(a) \tag{S16}$$

$$CO_2 + (a) = CO_2(a) \tag{S17}$$

$$O_2 + 2(a) = 2O(a) \tag{S18}$$

$$CHO(a) + O(a) = CO(a) + HO(a) \quad RDS_5 \tag{S19}$$

$$CH(a) + O(a) = CO(a) + H(a) \quad RDS_6 \tag{S20}$$

$$H(a) + O(a) = HO(a) + (a) \quad RDS_7 \tag{S21}$$

$$CO(a) + O(a) = CO_2(a) + (a) \quad RDS_8 \tag{S22}$$

In this mechanism, (a) indicates an empty active site. For each of the eight reactions comprising the reaction scheme, a catalytic cycle using the elemental steps (S1−S22) can be formulated. In each cycle, it is assumed that only one rate-determining step (RDS) exists and that the other steps are in "quasi-equilibrium". In all the cases, it is assumed that the surface reaction is the RDS. The reaction rate of each reaction in the proposed reaction scheme is determined by the reaction rate of the RDS in each catalytic cycle. The kinetic expressions were obtained on the basis of the Langmuir−Hinshelwood−Hougen−Watson theory and are as follows:

$$r_1 = \frac{k_1}{DEN^2}\frac{y_{Et}}{y_{CH_4}y_{H_2}^{1/2}}$$

$$r_2 = \frac{k_2}{DEN^2}\frac{y_{Et}y_{H_2O}}{y_{CH_4}y_{H_2}}$$

$$r_{WGS} = \frac{k_{WGS}}{DEN^2}\frac{y_{CO}y_{H_2O}}{y_{H_2}^{1/2}}\left[1 - \frac{1}{K_{WGS}}\frac{y_{CO_2}y_{H_2}}{y_{CO}y_{H_2O}}\right]$$

$$r_{MSR} = \frac{k_{MSR}}{DEN^2}\frac{y_{CH_4}y_{H_2O}}{y_{H_2}^{2}}\left[1 - \frac{1}{K_{MSR}}\frac{y_{CO}y_{H_2}^{3}}{y_{CH_4}y_{H_2O}}\right]$$

$$r_5 = \frac{k_5}{DEN_1^2}\frac{y_{Et}y_{O_2}^{1/2}}{y_{CH_4}y_{H_2}^{1/2}}$$

$$r_6 = \frac{k_6}{DEN_1^2}\frac{y_{CH_4}y_{O_2}^{1/2}}{y_{H_2}^{3/2}}$$

$$r_7 = \frac{k_7}{DEN_1^2}y_{H_2}^{1/2}y_{O_2}^{1/2}$$

$$r_8 = \frac{k_8}{DEN_1^2}y_{CO}y_{O_2}^{1/2}$$

$$DEN = 1 + K_{Et}y_{Et} + K_{Etx}\frac{y_{Et}}{y_{H_2}^{1/2}} + K_{Ac}\frac{y_{Et}}{y_{H_2}} + K_{CHO}\frac{y_{Et}}{y_{H_2}^{1/2}y_{CH_4}} + K_{CH_2}\frac{y_{CH_4}}{y_{H_2}} + K_{CH}\frac{y_{CH_4}}{y_{H_2}^{3/2}} + K_{CH_3}\frac{y_{CH_4}}{y_{H_2}^{1/2}} + K_{H_2O}y_{H_2O} + K_{H_2O}\frac{y_{H_2O}}{y_{H_2}^{1/2}} + K_H y_{H_2}^{1/2} + K_{CH_4}y_{CH_4} + K_{CO}y_{CO} + K_{CO_2}y_{CO_2}$$

$$DEN_1 = 1 + K_{Et}y_{Et} + K_{Etx}\frac{y_{Et}}{y_{H_2}^{1/2}} + K_{Ac}\frac{y_{Et}}{y_{H_2}} + K_{CHO}\frac{y_{Et}}{y_{H_2}^{1/2}y_{CH_4}} + K_{CH_2}\frac{y_{CH_4}}{y_{H_2}} + K_{CH}\frac{y_{CH_4}}{y_{H_2}^{3/2}} + K_{CH_3}\frac{y_{CH_4}}{y_{H_2}^{1/2}} + K_{H_2O}y_{H_2O} + K_{H_2O}\frac{y_{H_2O}}{y_{H_2}^{1/2}} + K_H y_{H_2}^{1/2} + K_{CH_4}y_{CH_4} + K_{CO}y_{CO} + K_{CO_2}y_{CO_2} + K_O y_{O_2}^{1/2}$$

It must be noted that the r_1−r_4 expressions, related to the ESR, have the same denominator (DEN), and the r_5−r_8 expressions, related to the EPO, have another denominator (DEN_1). This is because the balance of active sites has now added a new species, the adsorbed oxygen, which results in a new parameter and a new term in the denominator.

3.6. Parameter Fitting. To obtain activation energies and adsorption enthalpies, the software Matlab was used. The number of data points used for the parameter adjustment was 246, and the corresponding variable levels were inlet compositions, temperature, and space time.

Table 5 shows the values of activation energies and adsorption enthalpies calculated. It was verified that activation energies have positive values and adsorption enthalpies have negative values. When comparing the values of the activation energies obtained previously in the reforming of ethanol with the same catalyst,[22] it can be seen that those corresponding to methane steam reforming, WGSR, ethanol decomposition, and ethanol steam reforming are very similar. The H_2 mole fraction determined with the model vs experimental mole fraction is shown in Figure 11. It can be seen that the fit is satisfactory for most of the events.

4. CONCLUSIONS

This work studied the oxidative steam reforming of ethanol on a $Rh(1\%)/MgAl_2O_4/Al_2O_3$ catalyst. This catalyst showed excellent selectivity for the production of hydrogen and very good stability. From the product distribution analysis. the reaction scheme was obtained. It was concluded that at low temperatures and low space times. oxidation reactions prevail over reforming reactions. Ethanol partial oxidation was also studied. and the same reaction scheme was obtained.

dx.doi.org/10.1021/ie500445u | Ind. Eng. Chem. Res. 2014, 53, 15348−15356

Table 5. Activation Energy (E_a) or Adsorption Enthalpy (ΔH) and Each Standard Deviation (σ)

	$E_a/\Delta H$ (J/mol)	σ
r_1	1.69×10^4	2.34×10^2
r_2	1.08×10^5	2.36×10^4
r_{WGS}	1.95×10^5	1.11×10^4
$_{SMR}r_{SMR}$	4.68×10^5	8.12×10^4
r_5	4.91×10^4	1.81×10^2
r_6	1.33×10^4	2.32×10^2
r_7	1.87×10^4	1.11×10^2
r_8	2.55×10^4	8.37×10^1
Et	-1.04×10^5	1.90×10^4
Etx	-1.25×10^5	4.71×10^4
Ac	-2.57×10^4	3.18×10^3
CHO	-1.30×10^4	3.13×10^3
CH_2	-4.32×10^5	1.26×10^4
CH	-2.87×10^5	7.55×10^4
CH_3	-4.77×10^5	9.08×10^3
H_2O	-4.01×10^5	8.20×10^4
OH	-1.58×10^5	7.18×10^3
H	-4.19×10^5	8.12×10^4
O	-6.45×10^4	1.56×10^3
CH_4	-5.33×10^4	5.72×10^3
CO	-2.91×10^5	5.60×10^4
CO_2	-2.20×10^5	8.12×10^3

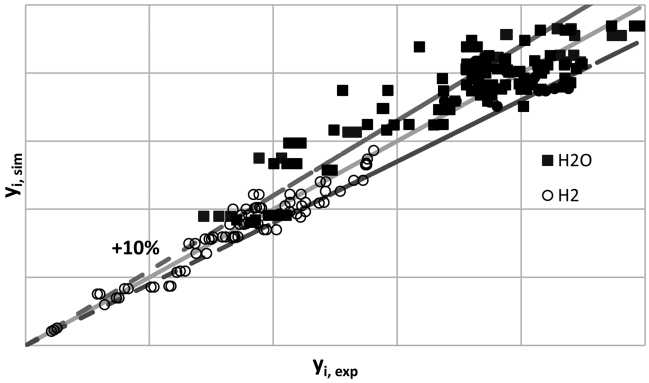

Figure 11. Parity graphic for H_2 and H_2O under different experimental conditions.

A reaction mechanism with 22 elementary steps was proposed, and the kinetic parameters were calculated considering that the rate-determining step is, in all the cases, the surface reaction. Activation energies of the eight reactions proposed and adsorption enthalpies for each compound involved were obtained.

Finally, taking into account the values of the kinetic parameters presented in Table 5 and the values of the molar fractions of the substances involved, simplified kinetic expressions for each of the eight reactions can be obtained.

■ ASSOCIATED CONTENT

Supporting Information

The procedure for the estimation of kinetic and adsorption parameters. This material is available free of charge via the Internet at http://pubs.acs.org.

■ AUTHOR INFORMATION

Corresponding Author

*Tel. +541145763211. E-mail: miguel@di.fcen.uba.ar.

Notes

The authors declare no competing financial interest.

■ ACKNOWLEDGMENTS

The authors thank CONICET, ANPCyT, and the University of Buenos Aires for financial support and Peruilh Foundation for Cecilia Graschinsky's scholarship. The team "Catalysis by Metals" from IC2MP (UMR 7285 University of Poitiers/CNRS) is gratefully acknowledged for providing the Rh catalyst for this study.

■ REFERENCES

(1) Holladay, J. D.; Hu, J.; King, D. L.; Wang, Y. An overview of hydrogen production technologies. *Catal. Today* **2009**, *139*, 244−260.
(2) Laborde, M.; Rubiera, F. *La energía del hidrógeno*; CYTED ed.s: Buenos Aires, 2010.
(3) Comas, J.; Mariño, F.; Laborde, M.; Amadeo, N. Bio-ethanol steam reforming on Ni/Al_2O_3 catalyst. *Chem. Eng. J.* **2004**, *98*, 61−68.
(4) Comas, J.; Dieuzeide, L.; Baronetti, G.; Laborde, M.; Amadeo, N. Methane steam reforming and ethanol steam reforming using a Ni(II)-Al(III) catalyst prepared from lamellar double hydroxides. *Chem. Eng. J.* **2006**, *118*, 11−15.
(5) Lima da Silva, A.; de Fraga Malfatti, C.; Müller, I. Thermodynamic analysis of ethanol steam reforming using Gibbs energy minimization method: A detailed study of the conditions of carbon deposition. *Int. J. Hydrogen Energy* **2009**, *34*, 4321−4330.
(6) Liu, S.; Zhang, K.; Fang, L.; Li, Y. Thermodynamic analysis of hydrogen production from oxidative steam reforming of ethanol. *Energy Fuels* **2008**, *22*, 1365−1370.
(7) Rabenstein, G.; Hacker, V. Hydrogen for fuel cells from ethanol by steam-reforming, partial-oxidation and combined auto-thermal reforming: A thermodynamic analysis. *J. Power Sources* **2008**, *185*, 1293−1304.
(8) Mas, V.; Bergamini, M. L.; Baronetti, G.; Amadeo, N.; Laborde, M. A. A kinetic study of ethanol steam reforming using a nickel based catalyst. *Top. Catal.* **2008**, *51*, 39−48.
(9) Graschinsky, C.; Giunta, P.; Amadeo, N.; Laborde, M. Thermodynamic analysis of hydrogen production by autothermal reforming of ethanol. *Int. J. Hydrogen Energy* **2012**, *37*, 10118−10124.
(10) Wang, W.; Wang, Y. Thermodynamic analysis of hydrogen production via partial oxidation of ethanol. *Int. J. Hydrogen Energy* **2008**, *33*, 5035−5044.
(11) Cavallaro, S. Ethanol steam reforming on Rh/Al_2O_3 catalysts. *Energy Fuels* **2000**, *14*, 1195−1199.
(12) Salge, J. R.; Deluga, G. A.; Schmidt, L. D. Catalytic partial oxidation of ethanol over noble metal catalysts. *J. Catal.* **2005**, *235*, 69−78.
(13) Biswas, P.; Kunzru, D. Oxidative steam reforming of ethanol over $Ni/CeO_2−ZrO_2$ catalyst. *Chem. Eng. J.* **2008**, *136*, 41−49.
(14) Fierro, V.; Akdim, O.; Provendier, H.; Mirodatos, C. Ethanol oxidative steam reforming over Ni-based catalysts. *J. Power Sources* **2005**, *145*, 659−666.
(15) Liguras, D.; Goundani, K.; Verykios, X. Production of hydrogen for fuel cells by catalytic partial oxidation of ethanol over structured Ru catalysts. *J. Power Sources* **2004**, *130*, 30−37.
(16) de Lima, S.; da Silva, A.; da Costa, L.; Assaf, J.; Jacobs, G.; Davis, B.; Mattos, L.; Noronha, F. Evaluation of the performance of Ni/La_2O_3 catalyst prepared from $LaNiO_3$ perovskite-type oxides for the production of hydrogen through steam reforming and oxidative steam reforming of ethanol. *Appl. Catal., A* **2010**, *377*, 181−190.
(17) Frusteri, F.; Freni, S.; Chiodo, V.; Donato, S.; Bonura, G.; Cavallaro, S. Steam and auto-thermal reforming of bio-ethanol over MgO and CeO_2 Ni supported catalysts. *Int. J. Hydrogen Energy* **2006**, *31*, 2193−2199.
(18) Huang, L.; Xie, J.; Chu, W.; Chen, R.; Chu, D.; Hsu, A. Iron-promoted nickel-based catalysts for hydrogen generation via auto-thermal reforming of ethanol. *Catal. Commun.* **2009**, *10*, 502−508.

(19) Gutierrez, A.; Karinen, R.; Airaksinen, S.; Kaila, R.; Krause, A. Autothermal reforming of ethanol on noble metal catalysts. *Int. J. Hydrogen Energy* **2011**, *36*, 8967−8977.
(20) Peela, N.; Kunzru, D. Oxidative steam reforming of ethanol over Rh-based catalysts in a micro-channel reactor. *Int. J. Hydrogen Energy* **2011**, *36*, 3384−3396.
(21) Srisiriwat, N.; Therdthianwong, S.; Therdthianwong, A. Oxidative steam reforming of ethanol over Ni/Al_2O_3 catalysts promoted by CeO_2, ZrO_2 and CeO_2−ZrO_2. *Int. J. Hydrogen Energy* **2009**, *34*, 2224−2234.
(22) Graschinsky, C.; Laborde, M.; Amadeo, N.; Le Valant, A.; Bion, N.; Epron, F.; Duprez, D. Ethanol steam reforming over Rh(1%)-$MgAl_2O_4/Al_2O_3$: A kinetic study. *Ind. Eng. Chem. Res.* **2010**, *49*, 12383−12389.
(23) Aupretre, F.; Descorme, C.; Duprez, D.; Casanave, D.; Uzio, D. Ethanol steam reforming over $Mg_xNi_{1-x}Al_2O_3$ spinel oxide-supported Rh catalysts. *J. Catal.* **2005**, *233*, 464−477.
(24) Perry, R. H.; Green, D. W. *Chemical Engineers' Handbook*, 8th ed.; Mc Graw-Hill: New York, 2008.
(25) Rodriguez, M. L.; Ardissone, D. E.; Pedernera, M. N.; Borio, D. O. Influence of the oxygen feed distribution on the performance of a catalytic reactor for ATR of methane. *Catal. Today* **2010**, *156*, 246−253.
(26) Mattos, L.; Noronha, F. Hydrogen production for fuel cell applications by ethanol partial oxidation on Pt/CeO_2 catalysts: The effect of the reaction conditions and reaction mechanism. *J. Catal.* **2005**, *233*, 453−463.
(27) Costa, L.; Silva, A.; Borges, L.; Mattos, L.; Noronha, F. Partial oxidation of ethanol over Pd/CeO_2 and Pd/Y_2O_3 catalysts. *Catal. Today* **2008**, *138*, 147−151.
(28) de Lima, S.; da Cruz, I.; Jacobs, G.; Davis, B.; Mattos, L.; Noronha, F. Steam reforming, partial oxidation, and oxidative steam reforming of ethanol over $Pt/CeZrO_2$ catalyst. *J. Catal.* **2008**, *257*, 356−368.
(29) Silva, A.; Costa, L.; Barandas, A.; Borges, L.; Mattos, L.; Noronha, F. Effect of the metal nature on the reaction mechanism of the partial oxidation of ethanol over CeO_2-supported Pt and Rh catalysts. *Catal. Today* **2008**, *133*−*135*, 755−761.
(30) Gomez, M.; Arrua, L.; Abello, M. Kinetic study of partial oxidation of ethanol over VMgO catalyst. *Ind. Eng. Chem. Res.* **1997**, *36*, 3468−3472.
(31) Jiang, B.; Chang, R.; Lin, Y. Partial oxidation of ethanol to acetaldehyde over $LaMnO_3$-based perovskites: A kinetic study. *Ind. Eng. Chem. Res.* **2013**, *52*, 37−42.
(32) Diehm, C.; Kaltschmitt, T.; Deutschmann, O. Hydrogen production by partial oxidation of ethanol/gasoline blends over Rh/Al_2O_3. *Catal. Today* **2012**, *197*, 90−100.
(33) Hebben, N.; Diehm, C.; Deutschmann, O. Catalytic partial oxidation of ethanol on alumina-supported rhodium catalysts: An experimental study. *Appl. Catal., A* **2010**, *388*, 225−231.
(34) Salge, J.; Deluga, G.; Schmidt, L. Catalytic partial oxidation of ethanol over noble metal catalysts. *J. Catal.* **2005**, *235*, 69−78.
(35) Beck, B.; Harth, M.; Hamilton, N.; Carrero, C.; Uhlrich, J.; Trunschke, A.; Shaikhutdinov, S.; Schubert, H.; Freund, H.; Schlögl, R.; Sauer, J.; Schomäcker, R. Partial oxidation of ethanol on vanadia catalysts on supporting oxides with different redox properties compared to propane. *J. Catal.* **2012**, *296*, 120−131.
(36) Au, C.; Wang, H. Mechanistic studies of methane partial oxidation to syngas over SiO_2-supported rhodium catalysts. *J. Catal.* **1997**, *167*, 337−345.
(37) Hofstad, K.; Hoebink, J.; Holmen, A.; Marin, G. Partial oxidation of methane to synthesis gas over rhodium catalysts. *Catal. Today* **1998**, *40*, 157−170.
(38) Ruckenstein, E.; Wang, H. Effect of support on partial oxidation of methane to synthesis gas over supported rhodium catalysts. *J. Catal.* **1999**, *187*, 151−159.